THE JOURNAL OF PHYSICAL CHEMISTRY C
A JOURNAL OF THE AMERICAN CHEMICAL SOCIETY

pubs.acs.org/JPCC

Article

Gas Transport across Carbon Nitride Nanopores: A Comparison of van der Waals Functionals against the Random-Phase Approximation

Mohammad Tohidi Vahdat, Davide Campi, Nicola Colonna, Nicola Marzari,* and Kumar Varoon Agrawal*

Cite This: *J. Phys. Chem. C* 2021, 125, 18896−18904

Read Online

ACCESS | Metrics & More | Article Recommendations | Supporting Information

ABSTRACT: C_2N is an ordered two-dimensional carbon nitride with a high density (1.7×10^{14} cm^{-2}) of 3.1 Å-sized nanopores, making it promising for high-flux gas sieving for energy-efficient He and H_2 purification. Herein, we discuss the accurate calculation of potential energy surfaces for He, H_2, N_2, and CO_2 across C_2N nanopores, to characterize the gas-sieving potential of C_2N. We compare the potential energy surface derived from density-functional theory calculations using five commonly used van der Waals (vdW) approximations. While all five functionals point that the C_2N nanopore yields He/N_2 and H_2/N_2 selectivities over 1000, adsorption energies and energy barriers vary remarkably depending on the approximation chosen. To make progress, we compare the calculations against the results from the adiabatic connection fluctuation dissipation theory, with random-phase approximation, known to be accurate in capturing vdW interactions. The comparison indicates that the interaction energy is less accurate with vdW density functional theory. On the other hand, more empirical corrections work reasonably well, a finding that we also confirm for another carbon nitride lattice, poly(triazine imide). Overall, we recommend these for screening carbon nitride materials for gas separation, but also comparing functionals with higher-order approaches when dealing with different materials.

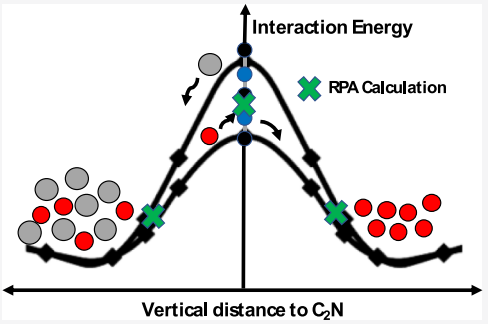

INTRODUCTION

Energy-efficient separation of He and H_2 is highly desirable for a number of medical, scientific, and energy applications.[1,2] Currently, He is recovered from various gas streams (CH_4, N_2, etc.) using cryogenic distillation,[3] while H_2 is primarily produced by steam reforming and is purified from cogenerated CO_2 by using CO_2-selective solvents or adsorbents.[4] These separation methods rely primarily on thermal energy, which makes them energy-intensive. As an alternative, high-performance membranes can reduce the energy footprint of these separation processes in remarkable ways.[5] Therefore, screening and identifying materials that can provide high-performance He and H_2 separation has become exceedingly important.[6−12]

Two-dimensional materials, especially those with a porous framework, are ideal for realizing membranes with an extremely thin selective layer. Among these, atom-thick materials hosting holes of the order of 3 Å (when measured with respect to the electron density) can be very attractive for high-permeance He and H_2 separation. In this case, gas transport across the selective layer is essentially given by just one crossing through the nanopore. The transport rate is then determined by the energy barrier at the nanopore[13,14] and the surface concentration of molecules, which, in turn, is determined by the adsorption energy at the pore. A prominent candidate for two-dimensional membranes is nanoporous single-layer graphene, where the lattice is etched to incorporate Å-scale nanopores for selective gas permeation.[15−17] Another promising class of atom-thick materials for He and H_2 separation is graphitic carbon nitrides. Several structures from this framework have intrinsic porosity with a pore size suitable for gas sieving. Among them, C_2N[18] and triazine- and heptazine-based carbon nitride [i.e., poly(triazine imide) or PTI[19,20] and poly(heptazine) imide or PHI[21] are very interesting. All of them are atom-thick, and possess a high pore density and ordered porosity. However, the pore size and shape are different, C_2N has a rounded pore, whereas PTI and PHI have triangular pores.

C_2N belongs to the family of graphitic carbon nitrides,[18] and hosts precisely shaped nanopores formed by the imide-linkage of six-membered sp^2-carbon rings (Figure 1a). As a result, its lattice is highly porous (pore density = 1.7×10^{14} cm^{-2}), which makes it promising for realizing large gas permeance.

Received: April 28, 2021
Revised: July 12, 2021
Published: August 18, 2021

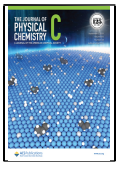

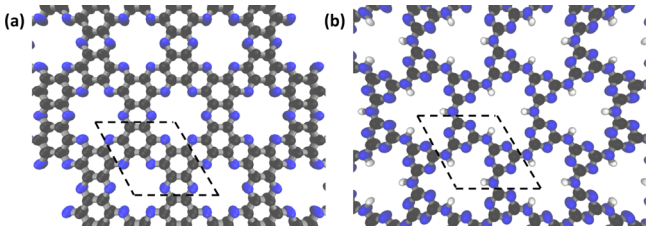

Figure 1. Ordered two-dimensional nanoporous structures of (a) C_2N and (b) PTI lattices. One can fit a circle with a diameter of 3.1 Å in C_2N nanopores. The PTI nanopore has the shape of an equilateral triangule in which a circle with a diameter of 3.4 Å can be fitted. The rhombi overlayed on their structure highlight the unit-cell for each structure.

The small electron density gap (~3.1 Å) in C_2N nanopores is highly suited for selective He and H_2 transport. In fact, several molecular simulation studies have indicated that only small gas molecules (He[22] and H_2[23]) can cross the C_2N nanopore with a low energy barrier. As a result, high He/CH_4 and H_2/N_2 selectivities can be achieved from the C_2N nanopores. Using van der Waals (vdW) density functional theory (DFT) calculations, Zhu et al.[22] estimated a low energy barrier (0.13 eV) for He and much larger energy barriers for N_2 (0.87 eV) and CH_4 (2.03 eV). This difference is large enough to deliver an exceptionally high gas-pair selectivity. Using classical molecular dynamics simulations, the same authors predicted a large He permeance (10^7 gas permeance units or GPU; 1 GPU = 3.35×10^{-10} mol m^{-2} s^{-1} Pa^{-1}) at 300 K. This permeance is several orders of magnitude higher than those of commercial membranes for He separation. In a separate DFT study focusing on H_2 transport across C_2N, Xu et al.[23] estimated energy barriers of 0.18, 0.72, and 1.05 eV for H_2, CO_2, and CO, respectively, indicating that C_2N blocks CO_2 and CO transport, and selectively permeates H_2. These molecular dynamic simulations also predicted an attractive H_2 permeance of 10^6 GPU. Such studies underscore the high impact that C_2N nanopores can have for an efficient separation of He and H_2.

We note that the vdW-DFT literature on gas transport across C_2N nanopores is not consistent. Widely different energy barriers for CO_2 have been reported, from 0.66[22] to 0.72[23] and 1.121 eV.[24] Additionally, widely different minimum energy pathways have also been reported. For example, Xu et al.[23] and Zhu et al.[22] showed that the repulsive interaction between CO_2 and the C_2N monolayers is maximized when the C atom of CO_2 arrives at the center of the pore. In contrast, Deng et al.[24] concluded that the maximum repulsive interaction occurs when an O atom of CO_2 is at the center of the pore. These differences are significant and raise questions on the accuracy of the vdW-DFT methods used to calculate the gas−lattice interactions. The role of vdW approximations in these studies is of particular interest. For example, Xu et al.[23] and Deng et al.[24] used vdW-DFT,[25] while Zhu et al.[22] used a semiempirical Grimme-D2 correction.[26] Interestingly, the Grimme approach[27] has also been used to study the adsorption and desorption of CO_2 on the surface of a C_2N monolayer.[28] In addition to the aforementioned studies, vdW-DF2[29] was used in the studies involving the electronic structure calculation of C_2N by Guan et al.[30] and Bai et al.[31]

Here, we systematically investigate the influence of five vdW approximations [vdW-DF2, Grimme-D2, Grimme-D3, revised version of Vydrov and van Voorhis functional (rVV10), and Tkatchenko−Scheffler (TS)] on the interaction of gases with the C_2N lattice to predict the potential energy surface (PES) of He, H_2, CO_2, and N_2 on a C_2N nanopore. We compare these calculations using a more accurate technique, that is, the exact exchange (EXX) in conjugation with random-phase approximation (RPA) to show that the Grimme-D2, Grimme-D3, and TS approaches work reasonably well, whereas vdW-DF2 and rvv10 either overestimate or underestimate the interaction energy. This observation is also confirmed for another promising graphitic carbon nitride material, poly(triazine imide) or PTI. Overall, we argue that Grimme-D2, Grimme-D3, and TS are good choices to screen carbon nitride materials for gas separation.

METHODS AND MODELS

The vdW-DFT calculations are performed using the Quantum ESPRESSO.[32,33] For the plane wave expansion of the wavefunctions, an energy cutoff of 60 Ry is used. A 2 × 2 supercell is used to decouple in-plane molecule−molecule interactions. The Brillouin zone is sampled with a uniform 6 × 6 × 1 unshifted *k*-point grids. To prevent any interactions among adjacent sheets, a vacuum region of 40 Å is used in the *z*-direction. Calculations are performed with ultrasoft pseudopotentials[34,35] and a kinetic energy cutoff of 480 Ry on the charge density. Five different dispersion corrections are used to include the contributions of dispersion interactions: vdW-DF2,[29] Grimme-D2,[26] Grimme-D3,[36] rVV10,[37,38] and TS.[39] Because TS has not been implemented with ultrasoft pseudopotentials in Quantum ESPRESSO, TS calculations are carried out with norm-conserving pseudopotentials,[40] using an energy cutoff of 100 Ry for the wavefunctions.

We compare these vdW-DFT calculations using the adiabatic connection fluctuation−dissipation theorem (ACFDT) framework.[41,42] We obtain total energies with EXX/RPA, which is known to be accurate in capturing vdW interactions, and used it to find the binding energies for different types of molecules.[43−46] The EXX/RPA calculations are performed using the implementation of the ACFDT formalism in the Quantum ESPRESSO distribution.[32,46,47] Because the computational resources required for EXX/RPA-based calculations are significantly higher than those needed using conventional DFT, additional convergence tests are carried out (Figure S2) to use EXX/RPA in a more efficient manner. The PES of molecules is explored as a function of the relaxation of molecules (Figure S2a), supercell size (Figure S2b), the density of the *k*-point grids (Figure S2c), the types of pseudopotentials (norm-conserving pseudopotential and ultrasoft pseudopotential, Figure S2d), and the cutoff values (Figure S2e). We show that EXX/RPA calculations on the gas−lattice systems considered in this study can be performed on a unit-cell using norm-conserving pseudopotential and sampling only at the Γ-point.

In this work, we use the EXX/RPA as an accurate and state-of-the-art technique to compare with our vdW-functional calculations. However, it is worth mentioning that the EXX/RPA has its own limitations that have been addressed in several ways and at different levels of sophistication. These include semilocal and non-local corrections[48,49] in order to describe short-range correlations properly, the use of improved kernel from TDDFT such as the renormalized adiabatic-LDA kernel[50,51] or the exact-exchange kernel[52−54] to describe better the density−density response function, or corrections based on many-body perturbation theory such as the screened-second order exchange[55−57] or the single-excitation correction.[58,59]

https://doi.org/10.1021/acs.jpcc.1c03822
J. Phys. Chem. C 2021, 125, 18896−18904

We also mention that all these corrective schemes have also been applied in a range-separated framework,[60,61] where only the long-range behavior of the RPA (and beyond schemes) is retained. In contrast, the short-range behavior is replaced by the one from semilocal or hybrid functionals. It has recently been shown that important effects beyond the dipole approximation typical of the RPA can be included within the many-body dispersion framework[62] by accounting for the dipole-correlated Coulomb singles,[63] which turns out to be particularly relevant in supramolecular systems and under nanoconfinement.

RESULTS AND DISCUSSION

Both C_2N and PTI have two-dimensional hexagonal lattices. To find the minimum energy configuration (lattice parameters), we relaxed the framework of C_2N and PTI using the five vdW approximations (vdW-DF2, Grimme-D2, Grimme-D3, TS, and rVV10) considered in this work. The relaxed lattice parameters (Table 1) go from 8.309 to 8.331 Å for C_2N and 8.638 to 8.673 Å for PTI, in agreement with the literature.[22,23,64] Next, we analyze the effective pore size for gas transport in these two lattices. The C_2N nanopores are somewhat round in shape. The effective pore size is determined by the six N atoms (blue atoms in Figure 1a) protruding in the nanopore. One can fit a circle with a diameter of 3.1 Å in this nanopore. On the other hand, the PTI nanopore has a triangular shape (Figure 1b), where one can fit a circle with a diameter of 3.4 Å. Next, we systematically investigate the role of the five vdW approximations in the gas−lattice interactions.

Table 1. Relaxed C_2N and PTI Lattice Parameters Using the Five vdW Approximations

vdW dispersion correction	C_2N lattice parameter (Å)	PTI lattice parameter (Å)
vdW-DF2	8.309	8.638
Grimme-D2	8.318	8.642
Grimme-D3	8.316	8.645
TS	8.317	8.647
rVV10	8.331	8.673

Constrained relaxation calculations are performed to study the interactions of He, H_2, CO_2, and N_2 with the nanoporous lattice as a function of the distance between the molecule and the lattice. For this, the lattice is placed in the $x-y$ plane at $z = 0$, and the gas molecule is placed at a certain distance along the z-direction. The center of mass of the molecule is fixed in the z-direction, but the molecule is allowed to relax in the $x-y$ plane. In this way, the molecule has the freedom to move in x and y directions to minimize the potential at a given distance from the lattice. Convergence thresholds of 2×10^{-6} Ry and 10^{-4} Ry/Bohr for the total energy and forces, respectively, are used. An assumption of a flexible or a rigid lattice did not significantly change the PES (Figure S1); therefore, we carried out the simulations using the rigid lattice.

To investigate the minimum energy pathway for the gas transport through the nanopore, the interaction between the gas molecule and the lattice is calculated as follows

$$E_{int} = E_{gas+lattice} - E_{gas} - E_{lattice} \quad (1)$$

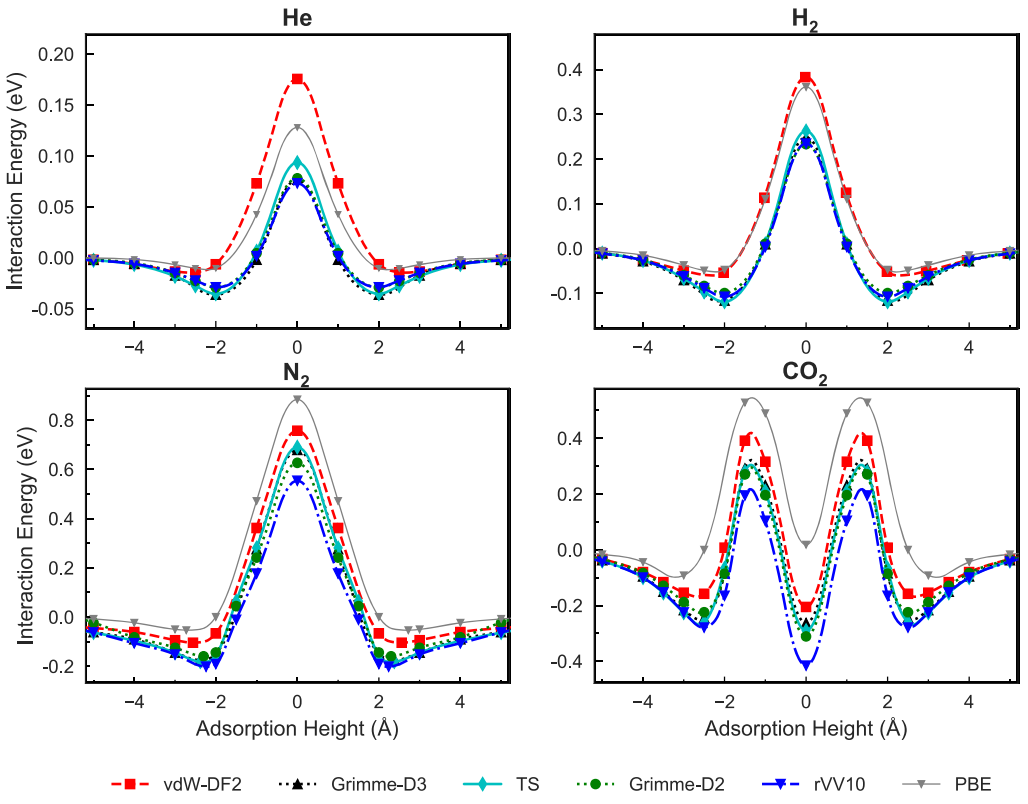

Figure 2. PESs of He (top left), H_2 (top right), N_2 (bottom left), and CO_2 (bottom right) on the C_2N lattice calculated using the five vdW approximations (vdW-DF2, Grimme-D2, Grimme-D3, rVV10, and TS) and the PBE functional.

https://doi.org/10.1021/acs.jpcc.1c03822
J. Phys. Chem. C 2021, 125, 18896−18904

where $E_{gas+lattice}$ is the total energy of the interacting system. E_{gas} and $E_{lattice}$ are the total energy of the gas and the lattice, respectively, when they are isolated and do not interact with each other. Because the PES for the gases considered in this study is simple enough (He is a single atom; H_2, N_2, and CO_2 are linear molecules), it is not required to carry out nudge elastic band calculations, and the constrained relaxation is sufficient.

The PES of the four gases on the C_2N lattice calculated using vdW-DF2, Grimme-D2, Grimme-D3, rVV10, and TS are shown in Figure 2, and are compared to the PES calculated using the Perdew–Burke–Ernzerhof (PBE) functional. Following observations are common to all PES:

(i) All four molecules prefer to adsorb on the C_2N lattice. The center of the mass of the adsorbed species lies in the centrosymmetric z-axis as shown in the Supporting Information Figure S3, in all four cases. The height of the adsorbed molecule above the pore, that is, the adsorption height, is listed in Table S1.

(ii) For the linear molecules (H_2, CO_2, and N_2), the most favorable configuration in the absorbed state is horizontal (configuration "1" in Figure 3).

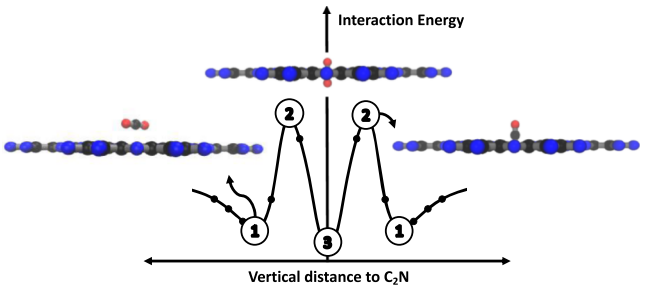

Figure 3. CO_2 configurations at three different z positions above the C_2N nanopore. In the first configuration, the CO_2 adsorbs horizontally above the nanopore. As it moves closer to the nanopore, it orients vertically (configuration "2"). Here, the O atom of the CO_2 is at the center of the nanopore. In this case, the interaction energy is governed by the repulsive interactions between O and the N atoms of the C_2N. Finally, CO_2 arrives at the center of the nanopore maintaining its vertical orientation (configuration "3"), where the C atom of CO_2 is at the center of the nanopore.

(iii) To fit inside the nanopore, the linear molecules prefer to orient vertically (configurations "2" and "3" in Figure 3). A vertical position of linear molecules inside the pore matches common intuition because if the gases were in the horizontal position, there would be a relatively larger overlap between the gas and the electron cloud of the pore edge.

(iv) The total energy of the system increases when the gases are brought close to the nanopore from the adsorbed state. For He, H_2, and N_2, the interaction energy increases monotonically as z decreases. Consequently, their PES has only one maximum at $z = 0$ (at the center of the nanopore). In contrast, the PES for CO_2 shows a maximum away from the nanopore ($z \neq 0$). This happens when the center of mass of CO_2 (C atom of CO_2) is at a distance of 1.1 Å from the nanopore (Figure 2). This is the position when the O atom of CO_2 is at the center of the nanopore (the configuration "2" in Figure 3).

The resulting M-shaped PES of CO_2 is unique. Deng et al.[24] also report an M-shaped PES with vdW-DF2 approximation, but the interaction energies are approximately 2.5-fold higher in their case. Later, by comparison with EXX/RPA calculations, we show that the M-shaped curve and energetics calculated in this study are indeed quite accurate. We also note that M-shaped PES for CO_2 has been reported for gas transport across a MoS_2 nanopore.[65]

Comparing several PES in Figure 2, it is evident that the PES calculated using the PBE functional underpredicts the attractive interactions between the molecule and the lattice compared to all other vdW functionals. Among the PES from the five vdW approximations, there is a significant difference in terms of the adsorption energy (E_{ads}, defined as the minimum E_{int}) and the energy barrier (E_{act}, defined as the difference in E_{int} at $z = 0$ and z corresponding to adsorption). E_{ads} values for He, H_2, N_2, and CO_2 are in the range of −0.01 to −0.03, −0.06 to −0.11, −0.10 to −0.20, and −0.16 to −0.28 eV, respectively. E_{act} values for He, H_2, and N_2 are in the range of 0.10–0.19, 0.33–0.44, and 0.76–0.87 eV, respectively.

The variation in E_{ads} and E_{act} from the five vdW approximations is expected to affect the He and H_2 separation performance. To understand the influence of vdW approximations on the He/N_2 and H_2/N_2 selectivities, we estimate the approximate selectivities by calculating the ratio of gas flux

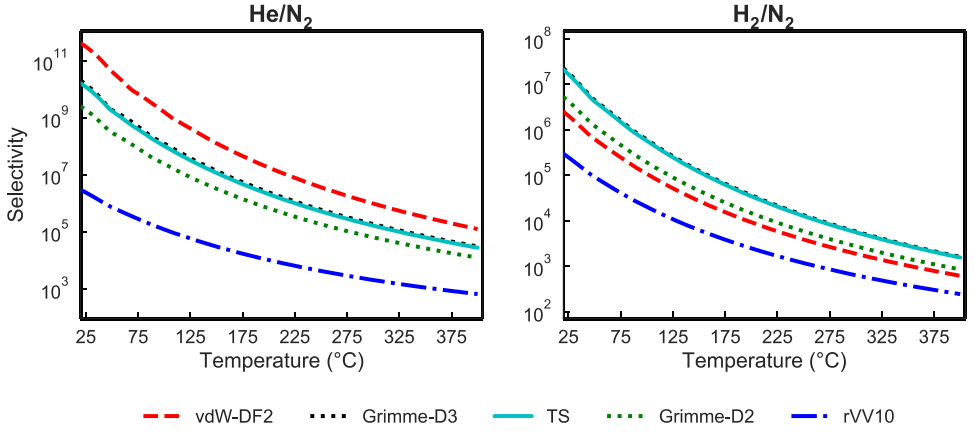

Figure 4. He/N_2 (left) and H_2/N_2 (right) selectivities from the C_2N nanopore as a function of temperature calculated with eq 3 using E_{act} and E_{ads} from the five vdW approximations.

https://doi.org/10.1021/acs.jpcc.1c03822
J. Phys. Chem. C 2021, 125, 18896−18904

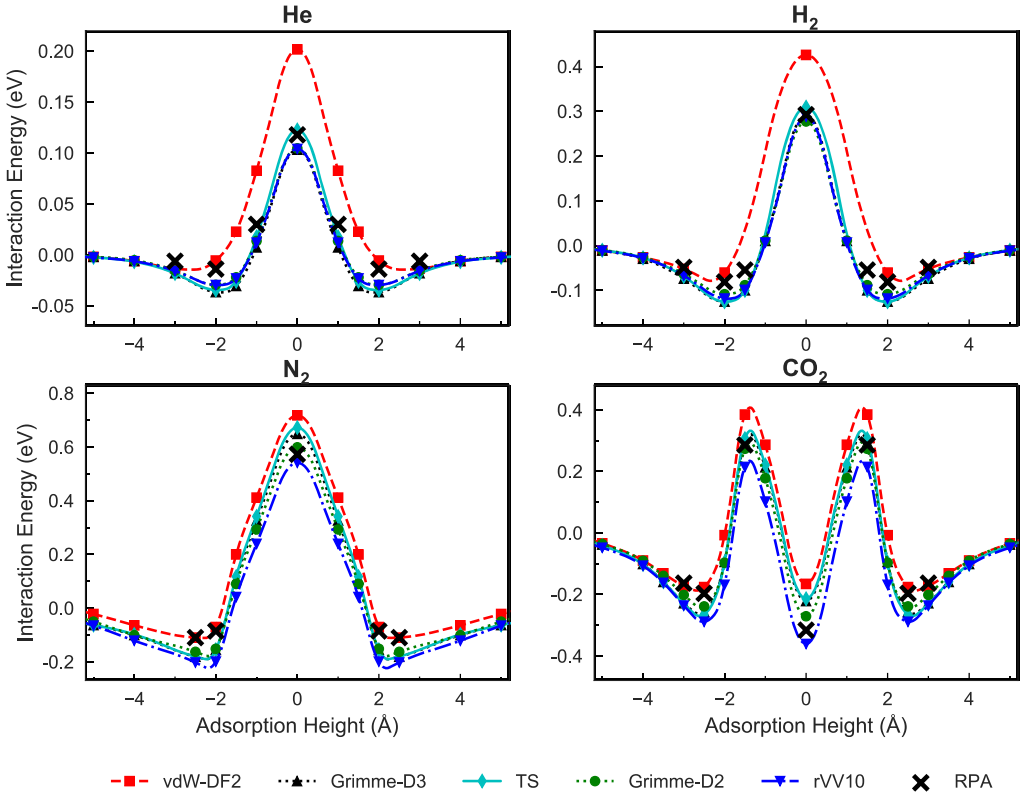

Figure 5. PESs of He, H_2, N_2, and CO_2 on a C_2N monolayer with different vdW approximations, vdW-DF2, Grimme-D2, Grimme-D3, rVV10, and TS. vdW-DFT calculations are compared against the results calculated with the EXX/RPA method.

(eq 2). Briefly, the gas flux, J, through a nanopore of commensurate size can be obtained by the transition-state theory, which yields an Arrhenius-type relationship to the flux (eq 2), where the pre-exponential factor, A, represents an entropic loss of the gas upon adsorption.[66] Given that (i) the energy barrier differences between He (or H_2) and N_2 are quite significant in the present case, and (ii) the entropic terms for light gases are generally within an order of magnitude,[67,68] we can neglect the entropic contribution to estimate the selectivity (eq 3).

$$J_i \propto A\exp(-(E_{ads,i} + E_{act,i}))/RT) \quad (2)$$

$$S_{i/j} \sim \frac{\exp(-(E_{ads,i} + E_{act,i}))/RT)}{\exp(-(E_{ads,j} + E_{act,j}))/RT)} \quad (3)$$

$$A = \frac{1}{L}\sqrt{\frac{RT}{2\pi M}}\exp\left(\frac{\Delta S}{R}\right) \quad (4)$$

where $E_{ads,i}$ and $E_{ads,j}$ represent E_{ads} for molecules i and j, respectively. Similarly, $E_{act,i}$ and $E_{act,j}$ represent E_{act} for molecules i and j, respectively. R is the universal gas constant and T is the temperature. L is the half-peak width of the probability distribution of the gas along the transport path from the adsorbed phase to the center of the pore, ΔS is the corresponding entropy change, and M is the molecular weight of the gas. Based on this, an approximate gas-pair selectivity within the temperature range of 25−400 °C is presented in Figure 4. In general, all five vdW approximations predict that C_2N nanopore would yield extremely high H_2/N_2 and He/N_2 selectivities, which make C_2N highly promising for these separations. The selectivity reduces with temperature in all cases because the sum of E_{ads} and E_{act}, also known as apparent activation energy in the experimental studies, is higher for N_2 than those for He and H_2, because of much higher E_{act} for N_2.

The discrepancy between the predicted selectivities from the five vdW approximations is quite large, differing by several orders of magnitude (Figure 4). Having a reliable quantitative estimation of the selectivity is especially important for H_2/N_2 separation at high temperature, relevant to H_2 production for NH_3 synthesis,[69] where selectivities of 100 and 1000 can lead to a large difference in membrane process design. To understand which of these vdW approximations provide the most accurate description of PES, we compared our calculations using a more advanced technique, EXX/RPA, which is known to accurately capture dispersion interactions[43] (Figure 5). For example, EXX/RPA calculations have shown a good agreement with experimental data on physisorption energies for several molecules on various surfaces.[44−46,57,70−72]

By comparing PES from the five vdW approximations with the interaction energy data from EXX/RPA calculations, we can make the following observations:

(i) vdW-DF2 correctly predicts the adsorption energy but overpredicts the repulsive interaction energy at the center of the pore.
(ii) rVV10 overpredicts the gas−lattice attractive interactions. In some cases, it also underpredicts the repulsive interaction energy at the center of the pore.
(iii) Grimme-D2, Grimme-D3, and TS slightly underpredict the adsorption energy but correctly predict the repulsive interaction at the center of the pore.

The EXX/RPA calculations validate the M-shaped PES of CO_2 on the C_2N nanopore and confirm the argument by Deng et al.[24] We also hold the view that the maximum energy at configuration "2" is due to the strong repulsive interactions

https://doi.org/10.1021/acs.jpcc.1c03822
J. Phys. Chem. C 2021, 125, 18896−18904

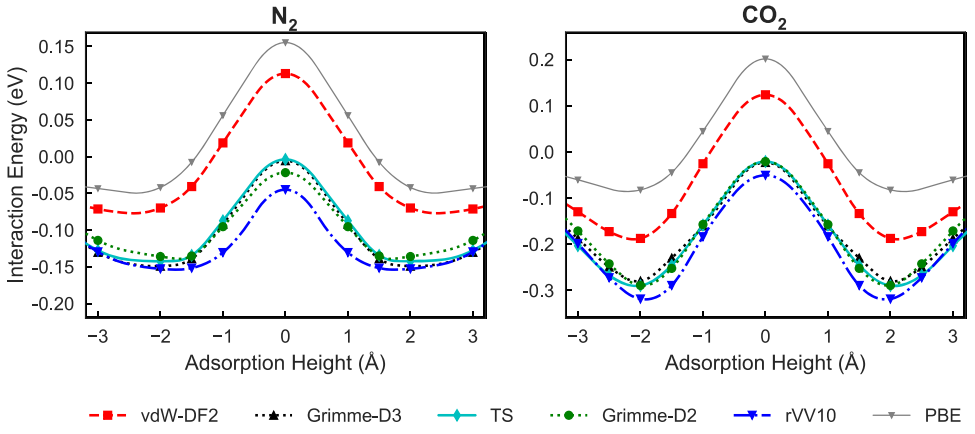

Figure 6. PESs of N_2 (left) and CO_2 (right) on a PTI nanopore using the five vdW approximations and the PBE functional.

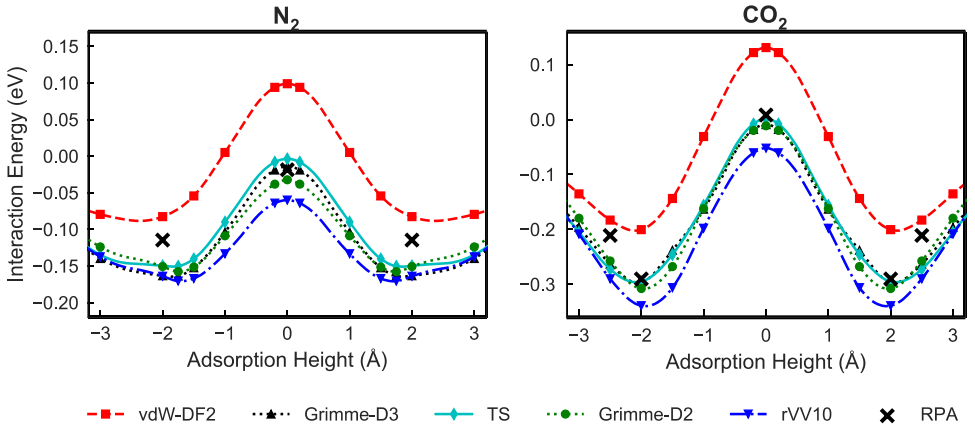

Figure 7. PESs of N_2 and CO_2 on a PTI monolayer with five vdW approximations compared against interaction energy data from EXX/RPA calculations.

between the O atom of CO_2 and the N atoms of the nanopore when CO_2 enters the nanopore in the vertical orientation with O atom arriving at the center of the pore. When the C atom of CO_2 finally arrives at the center of the pore (configuration "3"), the overall repulsive interaction reduces as a result of additional attraction interactions between the two O atoms of CO_2, positioned at the two sides of the nanopore, and the N atoms of the pore.

The above findings on the effect of vdW approximations on the PES of gas molecules motivated us to extend our analysis to PTI nanopores, another promising two-dimensional nanoporous material for high-flux gas separation. PTI nanopores are triangular in shape and are built from imide linkages between six triazine units (Figure 1). Our recent simulation study has shown that PTI nanopores can be used for sieving Kr (a kinetic diameter of 3.60 Å) from Xe (a kinetic diameter of 3.96 Å) with a large Kr/Xe separation selectivity and an attractive Kr permeance.[68] Here, we explore the PES of N_2 and CO_2 on PTI with the same set of vdW approximations as that used for C_2N.

Figure 6 compares six PES (one for each density functional) for N_2 and CO_2 on a PTI nanopore. Again, in all cases, in terms of the orientation of the gas molecules as a function of z, we observe a similar behavior to the one observed in the case of C_2N, that is, both N_2 and CO_2 prefer to adsorb in the horizontal configuration, whereas they prefer to enter the nanopore in the vertical configuration. Again, PBE underestimates the attractive interactions compared to all the other vdW functionals. We also observe quantitatively different interaction energies (E_{ads} and E_{act}) for the five vdW approximations. E_{ads} values for N_2 and CO_2 are in the range of −0.07 to −0.15 and −0.19 to −0.32 eV, respectively. E_{act} values for N_2 and CO_2 are in the range of 0.11−0.19 and 0.26−0.31 eV, respectively. We find it interesting that E_{act} for CO_2 is higher than that for N_2 given that CO_2 has a smaller kinetic diameter than N_2 (3.30 vs 3.64 Å). In the case of C_2N, the E_{act} value for CO_2 was smaller than that of N_2. This unexpected result in the case of PTI is likely rooted in the much stronger attractive interaction (or the potential well) of CO_2 at the adsorption site, which increases the energy barrier for CO_2 to hop to the transition state at the center of the pore. Next, to understand the accuracy of our calculations, we compare the PES with the interaction energy data from the EXX/RPA method.

Figure 7 compares the PES of N_2 and CO_2 on PTI obtained with vdW-DFT calculations with the interaction energy data from EXX/RPA calculations. Again, we can make a few general observations:

(i) vdW-DF2 underestimates the gas−lattice attractive interactions and ends up overpredicting the repulsive interaction energy at the center of the pore by a large margin.

(ii) rVV10 overestimates the gas−lattice attractive interactions and ends up underpredicting the repulsive interaction energy at the center of the pore by a large margin. However, the deviation from the EXX/RPA results is lower than that for vdW-DF2.

https://doi.org/10.1021/acs.jpcc.1c03822
J. Phys. Chem. C 2021, 125, 18896−18904

(iii) Grimme-D2, Grimme-D3, and TS slightly overestimate the attractive interactions for N_2 but correctly predict it for CO_2. They correctly predict the interaction at the center of the pore for both gases.

Overall, Grimme-D2, Grimme-D3, and TS lead to more accurate PES for PTI compared to those from vdW-DF2 and rVV10, consistent with the observations for C_2N, and therefore, can be considered a good choice for calculating gas−lattice interaction from a wider material database of the carbon nitride framework.

DISCUSSION ON THE LOWER ACCURACY OF VDW-DF2 AND RVV10

Our investigation on two promising carbon nitride materials for gas separation, C_2N and PTI, reveals that vdW-DFT calculations using Grimme-D2, Grimme-D3, and TS functionals are fairly accurate in capturing dispersion interactions. On the other hand, vdW-DF2 tends to underestimate the gas−lattice attractive interaction for both carbon nitride lattices. The same behavior is reported for carbon nanotubes when vdW-DF2 is used.[73] On the other hand, rVV10 tends to overestimate the attractive interaction. The relatively poor performance of rVV10 can be attributed to the negligence of the charge screening effect, which is known to be very important for anisotropic systems such as those considered in our study.[74,75] Moreover, it is known that the rVV10 performance improves when it is used with more "repulsive" semilocal functionals (those capturing the exchange repulsion).[74] Therefore, the PBE functionals might not be the best option to be paired with rVV10 (in this study, we used the PBE exchange−correlation functional for the sake of consistency).

CONCLUSIONS

This study illustrates the importance of capturing accurate vdW interactions for screening nanoporous materials for gas separation. We compared PES of He, H_2, N_2, and CO_2 across C_2N for five vdW approximations (Grimme-D2, Grimme-D3, rVV10, TS, and vdW-DF2), and showed that gas-pair selectivity changes significantly depending on the choice of the vdW approximation. By comparing vdW-DFT calculations against more accurate EXX/RPA calculations, we show that Grimme-D2, Grimme-D3, and TS are reliable choices to investigate carbon nitride nanopores for gas separation. We find a unique M-shaped PES for CO_2, which originates from initially repulsive to subsequently attractive interactions between the O atom of CO_2 and the N atom of the nanopore when CO_2 traverses the nanopore in the vertical orientation. The gas-pair selectivity estimates based on transition-state-theory confirm that C_2N is an excellent candidate for He/N_2 and H_2/N_2 separation, with selectivity estimated over 1000 over a wide range of temperatures.

The accuracy of vdW-DF2 and rvv10 might be affected by the anisotropic nature of the gas−lattice system. We note that the conclusions on the accuracy of Grimme-D2, Grimme-D3, and TS over vdW-DF2 and TS for carbon nitride frameworks remain to be verified for materials outside the carbon nitride family. The careful approach taken here for comparing the vdW approximations with EXX/RPA calculations can be applied to several other relevant materials, from nanoporous single-layer graphene to transition metal dichalcogenides and hexagonal boron nitride.

ASSOCIATED CONTENT

Supporting Information

The Supporting Information is available free of charge at https://pubs.acs.org/doi/10.1021/acs.jpcc.1c03822.

Exploring the influence of fixing the monolayer during the PES calculations; RPA convergence tests; N_2 molecule on top of the C_2N monolayer; adsorption height of H_2, He, N_2, and CO_2 on a C_2N monolayer; and vibrational frequency of adsorbed H_2 on the C_2N monolayer (PDF)

AUTHOR INFORMATION

Corresponding Authors

Nicola Marzari − *Theory and Simulation of Materials (THEOS) and National Centre for Computational Design and Discovery of Novel Materials (MARVEL), EPFL, CH-1015 Lausanne, Switzerland;* orcid.org/0000-0002-9764-0199; Email: nicola.marzari@epfl.ch

Kumar Varoon Agrawal − *Laboratory of Advanced Separations (LAS), École Polytechnique Fédérale de Lausanne (EPFL), CH-1950 Sion, Switzerland;* orcid.org/0000-0002-5170-6412; Email: kumar.agrawal@epfl.ch

Authors

Mohammad Tohidi Vahdat − *Laboratory of Advanced Separations (LAS), École Polytechnique Fédérale de Lausanne (EPFL), CH-1950 Sion, Switzerland; Theory and Simulation of Materials (THEOS) and National Centre for Computational Design and Discovery of Novel Materials (MARVEL), EPFL, CH-1015 Lausanne, Switzerland*

Davide Campi − *Theory and Simulation of Materials (THEOS) and National Centre for Computational Design and Discovery of Novel Materials (MARVEL), EPFL, CH-1015 Lausanne, Switzerland;* Present Address: Dipartimento di Scienza dei Materiali, Università di Milano-Bicocca, Via R. Cozzi 55, I-20125 Milano, Italy; orcid.org/0000-0002-6278-4352

Nicola Colonna − *Theory and Simulation of Materials (THEOS) and National Centre for Computational Design and Discovery of Novel Materials (MARVEL), EPFL, CH-1015 Lausanne, Switzerland; Laboratory for Neutron Scattering and Imaging (LNS), Paul Scherrer Institute (PSI), CH-5232 Villigen, Switzerland;* orcid.org/0000-0002-6106-6316

Complete contact information is available at: https://pubs.acs.org/10.1021/acs.jpcc.1c03822

Notes

The authors declare no competing financial interest.

ACKNOWLEDGMENTS

We thank our host institution, EPFL, for generous support. Parts of the work were funded by the Swiss National Science Foundation (Assistant Professor Energy Grant; grant no PYAPP2_173645). We thank the Swiss National Supercomputing Center, CSCS, for the allocation of computing resources (production projects s860 and s953). D.C. and N.M. acknowledge support from the MARVEL NCCR. D.C. acknowledges support from the EPFL Fellows program cofunded by Marie Sklodowska-Curie, Horizon 2020 grant agreement no. 66566.

REFERENCES

(1) Schrier, J. Helium Separation Using Porous Graphene Membranes. *J. Phys. Chem. Lett.* **2010**, *1*, 2284−2287.
(2) Marbán, G.; Valdés-Solís, T. Towards the hydrogen economy? *Int. J. Hydrogen Energy* **2007**, *32*, 1625−1637.
(3) Van Sciver, S. W. Helium Cryogenics, 2nd ed.; *International Cryogenics Monograph Series*; Springer: New York, 2012.
(4) Gallucci, F.; Fernandez, E.; Corengia, P.; van Sint Annaland, M. Recent Advances on Membranes and Membrane Reactors for Hydrogen Production. *Chem. Eng. Sci.* **2013**, *92*, 40−66.
(5) National Academies of Sciences, Engineering, and Medicine, Division on Earth and Life Studies, Board on Chemical Sciences and Technology, Committee on a Research Agenda for a New Era in Separation Science *A Research Agenda for Transforming Separation Science*; National Academies Press, 2019.
(6) Shan, M.; Xue, Q.; Jing, N.; Ling, C.; Zhang, T.; Yan, Z.; Zheng, J. Influence of Chemical Functionalization on the CO_2/N_2 Separation Performance of Porous Graphene Membranes. *Nanoscale* **2012**, *4*, 5477.
(7) Tao, Y.; Xue, Q.; Liu, Z.; Shan, M.; Ling, C.; Wu, T.; Li, X. Tunable Hydrogen Separation in Porous Graphene Membrane: First-Principle and Molecular Dynamic Simulation. *ACS Appl. Mater. Interfaces* **2014**, *6*, 8048−8058.
(8) Du, H.; Li, J.; Zhang, J.; Su, G.; Li, X.; Zhao, Y. Separation of Hydrogen and Nitrogen Gases with Porous Graphene Membrane. *J. Phys. Chem. C* **2011**, *115*, 23261−23266.
(9) Jiang, D.-e.; Cooper, V. R.; Dai, S. Porous Graphene as the Ultimate Membrane for Gas Separation. *Nano Lett.* **2009**, *9*, 4019−4024.
(10) Wu, T.; Xue, Q.; Ling, C.; Shan, M.; Liu, Z.; Tao, Y.; Li, X. Fluorine-Modified Porous Graphene as Membrane for CO_2/N_2 Separation: Molecular Dynamic and First-Principles Simulations. *J. Phys. Chem. C* **2014**, *118*, 7369−7376.
(11) Ambrosetti, A.; Silvestrelli, P. L. Gas Separation in Nanoporous Graphene from First Principle Calculations. *J. Phys. Chem. C* **2014**, *118*, 19172−19179.
(12) Zhang, Y.; Shi, Q.; Liu, Y.; Wang, Y.; Meng, Z.; Xiao, C.; Deng, K.; Rao, D.; Lu, R. Hexagonal Boron Nitride with Designed Nanopores as a High-Efficiency Membrane for Separating Gaseous Hydrogen from Methane. *J. Phys. Chem. C* **2015**, *119*, 19826−19831.
(13) Yuan, Z.; Govind Rajan, A.; Misra, R. P.; Drahushuk, L. W.; Agrawal, K. V.; Strano, M. S.; Blankschtein, D. Mechanism and Prediction of Gas Permeation through Sub-Nanometer Graphene Pores: Comparison of Theory and Simulation. *ACS Nano* **2017**, *11*, 7974−7987.
(14) Yuan, Z.; Misra, R. P.; Rajan, A. G.; Strano, M. S.; Blankschtein, D. Analytical Prediction of Gas Permeation through Graphene Nanopores of Varying Sizes: Understanding Transitions across Multiple Transport Regimes. *ACS Nano* **2019**, *13*, 11809−11824.
(15) Zhao, J.; He, G.; Huang, S.; Villalobos, L. F.; Dakhchoune, M.; Bassas, H.; Agrawal, K. V. Etching Gas-Sieving Nanopores in Single-Layer Graphene with an Angstrom Precision for High-Performance Gas Mixture Separation. *Sci. Adv.* **2019**, *5*, No. eaav1851.
(16) He, G.; Huang, S.; Villalobos, L. F.; Vahdat, M. T.; Guiver, M. D.; Zhao, J.; Lee, W. C.; Mensi, M.; Agrawal, K. V. Synergistic CO_2-Sieving from Polymer with Intrinsic Microporosity Masking Nanoporous Single-Layer Graphene. *Adv. Funct. Mater.* **2020**, *30*, 2003979.
(17) Huang, S.; Li, S.; Villalobos, L. F.; Dakhchoune, M.; Micari, M.; Babu, D. J.; Vahdat, M. T.; Mensi, M.; Oveisi, E.; Agrawal, K. V. Millisecond Lattice Gasification for High-Density CO2- and O2-Sieving Nanopores in Single-Layer Graphene. *Sci. Adv.* **2021**, *7*, No. eabf0116.
(18) Mahmood, J.; Lee, E. K.; Jung, M.; Shin, D.; Jeon, I.-Y.; Jung, S.-M.; Choi, H.-J.; Seo, J.-M.; Bae, S.-Y.; Sohn, S.-D.; et al. Nitrogenated Holey Two-Dimensional Structures. *Nat. Commun.* **2015**, *6*, 6486.
(19) Talukdar, M.; Behera, S. K.; Deb, P. Graphitic Carbon Nitride Decorated with $FeNi_3$ Nanoparticles for Flexible Planar Micro-Supercapacitor with Ultrahigh Energy Density and Quantum Storage Capacity. *Dalton Trans.* **2019**, *48*, 12137−12146.
(20) Talukdar, M.; Behera, S. K.; Bhattacharya, K.; Deb, P. Surface Modified Mesoporous G-C_3N_4@$FeNi_3$ as Prompt and Proficient Magnetic Adsorbent for Crude Oil Recovery. *Appl. Surf. Sci.* **2019**, *473*, 275−281.
(21) Wang, Y.; Gao, B.; Yue, Q.; Wang, Z. Graphitic Carbon Nitride (g-C_3N_4)-Based Membranes for Advanced Separation. *J. Mater. Chem. A* **2020**, *8*, 19133−19155.
(22) Zhu, L.; Xue, Q.; Li, X.; Wu, T.; Jin, Y.; Xing, W. C2N An Excellent Two-Dimensional Monolayer Membrane for He Separation. *J. Mater. Chem. A* **2015**, *3*, 21351−21356.
(23) Xu, B.; Xiang, H.; Wei, Q.; Liu, J. Q.; Xia, Y. D.; Yin, J.; Liu, Z. G. Two-Dimensional Graphene-like C_2N: An Experimentally Available Porous Membrane for Hydrogen Purification. *Phys. Chem. Chem. Phys.* **2015**, *17*, 15115−15118.
(24) Deng, S.; Hu, H.; Zhuang, G.; Zhong, X.; Wang, J. A Strain-Controlled C_2N Monolayer Membrane for Gas Separation in PEMFC Application. *Appl. Surf. Sci.* **2018**, *441*, 408−414.
(25) Dion, M.; Rydberg, H.; Schröder, E.; Langreth, D. C.; Lundqvist, B. I. Van der Waals Density Functional for General Geometries. *Phys. Rev. Lett.* **2004**, *92*, 246401.
(26) Grimme, S. Accurate Description of van der Waals Complexes by Density Functional Theory Including Empirical Corrections. *J. Comput. Chem.* **2004**, *25*, 1463−1473.
(27) Grimme, S. Semiempirical GGA-Type Density Functional Constructed with a Long-Range Dispersion Correction. *J. Comput. Chem.* **2006**, *27*, 1787−1799.
(28) Qin, G.-q.; Du, A.-j.; Sun, Q. Charge- and Electric-Field-Controlled Switchable Carbon Dioxide Capture and Gas Separation on a C_2N Monolayer. *Energy Technol.* **2018**, *6*, 205−212.
(29) Lee, K.; Murray, É. D.; Kong, L.; Lundqvist, B. I.; Langreth, D. C. Higher-Accuracy van der Waals Density Functional. *Phys. Rev. B: Condens. Matter Mater. Phys.* **2010**, *82*, 081101.
(30) Guan, Z.; Lian, C.-S.; Hu, S.; Ni, S.; Li, J.; Duan, W. Tunable Structural, Electronic, and Optical Properties of Layered Two-Dimensional C_2N and MoS_2 van der Waals Heterostructure as Photovoltaic Material. *J. Phys. Chem. C* **2017**, *121*, 3654−3660.
(31) Bai, Y.; Zhang, Q.; Xu, N.; Deng, K.; Kan, E. Efficient Carrier Separation and Band Structure Tuning of Two-Dimensional C_2N/GaTe van der Waals Heterostructure. *J. Phys. Chem. C* **2018**, *122*, 15892−15902.
(32) Giannozzi, P.; Baroni, S.; Bonini, N.; Calandra, M.; Car, R.; Cavazzoni, C.; Ceresoli, D.; Chiarotti, G. L.; Cococcioni, M.; Dabo, I.; et al. QUANTUM ESPRESSO: A Modular and Open-Source Software Project for Quantum Simulations of Materials. *J. Phys. Condens. Matter* **2009**, *21*, 395502.
(33) Giannozzi, P.; Andreussi, O.; Brumme, T.; Bunau, O.; Buongiorno-Nardelli, M.; Calandra, M.; Car, R.; Cavazzoni, C.; Ceresoli, D.; Cococcioni, M.; et al. Advanced Capabilities for Materials Modelling with Quantum ESPRESSO. *J. Phys. Condens. Matter* **2017**, *29*, 465901.
(34) Lejaeghere, K.; Bihlmayer, G.; Bjorkman, T.; Blaha, P.; Blugel, S.; Blum, V.; Caliste, D.; Castelli, I. E.; Clark, S. J.; Dal Corso, A.; et al. Reproducibility in Density Functional Theory Calculations of Solids. *Science* **2016**, *351*, aad3000.
(35) Prandini, G.; Marrazzo, A.; Castelli, I. E.; Mounet, N.; Marzari, N. Precision and Efficiency in Solid-State Pseudopotential Calculations. *npj Comput. Mater.* **2018**, *4*, 72.
(36) Grimme, S.; Antony, J.; Ehrlich, S.; Krieg, H. A Consistent and Accurate Ab Initio Parametrization of Density Functional Dispersion Correction (DFT-D) for the 94 Elements H-Pu. *J. Chem. Phys.* **2010**, *132*, 154104.
(37) Vydrov, O. A.; Van Voorhis, T. Nonlocal van der Waals Density Functional: The Simpler the Better. *J. Chem. Phys.* **2010**, *133*, 244103.
(38) Sabatini, R.; Gorni, T.; de Gironcoli, S. Nonlocal van der Waals Density Functional Made Simple and Efficient. *Phys. Rev. B: Condens. Matter Mater. Phys.* **2013**, *87*, 041108.

https://doi.org/10.1021/acs.jpcc.1c03822
J. Phys. Chem. C 2021, 125, 18896−18904

(39) Tkatchenko, A.; Scheffler, M. Accurate Molecular van der Waals Interactions from Ground-State Electron Density and Free-Atom Reference Data. *Phys. Rev. Lett.* **2009**, *102*, 073005.
(40) van Setten, M. J.; Giantomassi, M.; Bousquet, E.; Verstraete, M. J.; Hamann, D. R.; Gonze, X.; Rignanese, G.-M. The PseudoDojo: Training and Grading a 85 Element Optimized Norm-Conserving Pseudopotential Table. *Comput. Phys. Commun.* **2018**, *226*, 39−54.
(41) Langreth, D. C.; Perdew, J. P. The Exchange-Correlation Energy of a Metallic Surface. *Solid State Commun.* **1975**, *17*, 1425−1429.
(42) Langreth, D. C.; Perdew, J. P. Exchange-Correlation Energy of a Metallic Surface: Wave-Vector Analysis. *Phys. Rev. B: Solid State* **1977**, *15*, 2884−2901.
(43) Dobson, J. F.; Gould, T. Calculation of Dispersion Energies. *J. Phys. Condens. Matter* **2012**, *24*, 073201.
(44) Ren, X.; Rinke, P.; Scheffler, M. Exploring the Random Phase Approximation: Application to CO Adsorbed on Cu(111). *Phys. Rev. B: Condens. Matter Mater. Phys.* **2009**, *80*, 045402.
(45) Colonna, N.; Hellgren, M.; de Gironcoli, S. Molecular Bonding with the RPAx: From Weak Dispersion Forces to Strong Correlation. *Phys. Rev. B* **2016**, *93*, 195108.
(46) Lu, D.; Li, Y.; Rocca, D.; Galli, G. Ab Initio Calculation of van der Waals Bonded Molecular Crystals. *Phys. Rev. Lett.* **2009**, *102*, 206411.
(47) Nguyen, H.-V.; de Gironcoli, S. Efficient Calculation of Exact Exchange and RPA Correlation Energies in the Adiabatic-Connection Fluctuation-Dissipation Theory. *Phys. Rev. B: Condens. Matter Mater. Phys.* **2009**, *79*, 205114.
(48) Kurth, S.; Perdew, J. P. Density-Functional Correction of Random-Phase-Approximation Correlation with Results for Jellium Surface Energies. *Phys. Rev. B: Condens. Matter Mater. Phys.* **1999**, *59*, 10461−10468.
(49) Ruzsinszky, A.; Perdew, J. P.; Csonka, G. I. A Simple but Fully Nonlocal Correction to the Random Phase Approximation. *J. Chem. Phys.* **2011**, *134*, 114110.
(50) Olsen, T.; Thygesen, K. S. Beyond the Random Phase Approximation: Improved Description of Short-Range Correlation by a Renormalized Adiabatic Local Density Approximation. *Phys. Rev. B: Condens. Matter Mater. Phys.* **2013**, *88*, 115131.
(51) Olsen, T.; Thygesen, K. S. Accurate Ground-State Energies of Solids and Molecules from Time-Dependent Density-Functional Theory. *Phys. Rev. Lett.* **2014**, *112*, 203001.
(52) Görling, A. Exact Exchange Kernel for Time-dependent Density-functional Theory. *Int. J. Quantum Chem.* **1998**, *69*, 265−277.
(53) Hellgren, M.; von Barth, U. Exact-Exchange Kernel of Time-Dependent Density Functional Theory: Frequency Dependence and Photoabsorption Spectra of Atoms. *J. Chem. Phys.* **2009**, *131*, 044110.
(54) Colonna, N.; Hellgren, M.; de Gironcoli, S. Correlation Energy within Exact-Exchange Adiabatic Connection Fluctuation-Dissipation Theory: Systematic Development and Simple Approximations. *Phys. Rev. B: Condens. Matter Mater. Phys.* **2014**, *90*, 125150.
(55) Freeman, D. L. Coupled-Cluster Expansion Applied to the Electron Gas: Inclusion of Ring and Exchange Effects. *Phys. Rev. B: Solid State* **1977**, *15*, 5512−5521.
(56) Grüneis, A.; Marsman, M.; Harl, J.; Schimka, L.; Kresse, G. Making the Random Phase Approximation to Electronic Correlation Accurate. *J. Chem. Phys.* **2009**, *131*, 154115.
(57) Hellgren, M.; Colonna, N.; de Gironcoli, S. Beyond the Random Phase Approximation with a Local Exchange Vertex. *Phys. Rev. B* **2018**, *98*, 045117.
(58) Ren, X.; Tkatchenko, A.; Rinke, P.; Scheffler, M. Beyond the Random-Phase Approximation for the Electron Correlation Energy: The Importance of Single Excitations. *Phys. Rev. Lett.* **2011**, *106*, 153003.
(59) Klimeš, J.; Kaltak, M.; Maggio, E.; Kresse, G. Singles Correlation Energy Contributions in Solids. *J. Chem. Phys.* **2015**, *143*, 102816.
(60) Janesko, B. G.; Henderson, T. M.; Scuseria, G. E. Long-Range-Corrected Hybrids Including Random Phase Approximation Correlation. *J. Chem. Phys.* **2009**, *130*, 081105.
(61) Toulouse, J.; Gerber, I. C.; Jansen, G.; Savin, A.; Angyán, J. G. Adiabatic-Connection Fluctuation-Dissipation Density-Functional Theory Based on Range Separation. *Phys. Rev. Lett.* **2009**, *102*, 096404.
(62) Tkatchenko, A.; DiStasio, R. A.; Car, R.; Scheffler, M. Accurate and Efficient Method for Many-Body van der Waals Interactions. *Phys. Rev. Lett.* **2012**, *108*, 236402.
(63) Stöhr, M.; Sadhukhan, M.; Al-Hamdani, Y. S.; Hermann, J.; Tkatchenko, A. Coulomb Interactions between Dipolar Quantum Fluctuations in van der Waals Bound Molecules and Materials. *Nat. Commun.* **2021**, *12*, 137.
(64) Wang, Y.; Yang, Q.; Zhong, C.; Li, J. Graphene-like Poly(Triazine Imide) as N_2-Selective Ultrathin Membrane for Postcombustion CO_2 Capture. *J. Phys. Chem. C* **2016**, *120*, 28782−28788.
(65) Li, Y.; Linghu, Y.; Wu, C. Separation Properties of Porous MoS_2 Membranes Decorated with Small Molecules. *ACS Appl. Mater. Interfaces* **2020**, *12*, 20096−20102.
(66) Auerbach, S. M. Theory and Simulation of Jump Dynamics, Diffusion and Phase Equilibrium in Nanopores. *Int. Rev. Phys. Chem.* **2000**, *19*, 155−198.
(67) Blankenburg, S.; Bieri, M.; Fasel, R.; Müllen, K.; Pignedoli, C. A.; Passerone, D. Nanoporous Materials Porous Graphene as an Atmospheric Nanofilter. *Small* **2010**, *6*, 2266−2271.
(68) Vahdat, M. T.; Campi, D.; Colonna, N.; Villalobos, L. F.; Marzari, N.; Agrawal, K. V. Efficient Kr/Xe Separation from Triangular g-C_3N_4 Nanopores, a Simulation Study. *J. Mater. Chem. A* **2020**, *8*, 17747−17755.
(69) Perry, J. D.; Nagai, K.; Koros, W. J. Polymer Membranes for Hydrogen Separations. *MRS Bull.* **2006**, *31*, 745−749.
(70) Rohlfing, M.; Bredow, T. Binding Energy of Adsorbates on a Noble-Metal Surface: Exchange and Correlation Effects. *Phys. Rev. Lett.* **2008**, *101*, 266106.
(71) Ren, X.; Rinke, P.; Joas, C.; Scheffler, M. Random-Phase Approximation and Its Applications in Computational Chemistry and Materials Science. *J. Mater. Sci.* **2012**, *47*, 7447−7471.
(72) Rocca, D. Random-Phase Approximation Correlation Energies from Lanczos Chains and an Optimal Basis Set: Theory and Applications to the Benzene Dimer. *J. Chem. Phys.* **2014**, *140*, 18A501.
(73) Cai, X.; Xie, W. J.; Yang, Y.; Long, Z.; Zhang, J.; Qiao, Z.; Yang, L.; Gao, Y. Q. Structure of Water Confined between Two Parallel Graphene Plates. *J. Chem. Phys.* **2019**, *150*, 124703.
(74) Stöhr, M.; Van Voorhis, T.; Tkatchenko, A. Theory and Practice of Modeling van der Waals Interactions in Electronic-Structure Calculations. *Chem. Soc. Rev.* **2019**, *48*, 4118−4154.
(75) Hermann, J.; DiStasio, R. A.; Tkatchenko, A. First-Principles Models for van der Waals Interactions in Molecules and Materials: Concepts, Theory, and Applications. *Chem. Rev.* **2017**, *117*, 4714−4758.

https://doi.org/10.1021/acs.jpcc.1c03822
J. Phys. Chem. C 2021, 125, 18896−18904